VSC-driven Modelling for Soft Open Points and Battery Energy Storage Systems to Balance Three-phase Distribution Networks with Phase-specific Dispatching

Chengwei Lou, Ran Zhao, Hangxing Zhang, Lu Zhang, *Senior Member, IEEE*, Wei Tang, *Member, IEEE*, Jin Yang, *Senior Member, IEEE*, Linjuan Zhang

***Abstract*—This paper presents an advanced framework utilizing Voltage Source Converters (VSC) for modeling soft open points (SOPs) and battery energy storage systems (BESSs) to actively balance three-phase distribution networks, addressing the phase imbalance posed by the rise in renewable energy and distributed generation. Unlike traditional models focusing mainly on AC capacity constraints, this model delves into the DC-link complications, enabling a thorough examination of the interactions among active and reactive power, and the voltage levels on both AC and DC sides of the VSCs. The relationship between Pulsewidth Modulation (PWM) control configurations and VSC power outputs is outlined, facilitating enhanced control across both sides of the converters. This, additionally, improves cross-phase power transfer via SOPs and better three-phase balancing. The model also integrates the cooperative functionality of VSC-driven BESS to maintain phase balance. Phase-Specific Dispatching (PSDs) is introduced to flexibly allocate individual loads to distinct phases. An algorithm harmonizes the VSC-driven modeling SOPs and BESS with PSDs, improving computational efficiency for power flow and phase balance management. The proposed model significantly aids in reducing losses and enhancing three-phase power balancing, as shown by the findings.**

***Index Terms*—Active distribution network, optimal power flow, soft open points, battery energy storage systems, three-phase VSC-driven modelling, Benders decomposition**

NOMENCLATURE

Parameters

$S_{rated,i}$	Rated capacity of BESS at bus i
Δr_i^{φ}	Ratio change per tap
ϵ	Pre-defined tolerance
$\overline{v_i}$	Upper limit of voltage at bus i
σ	A positive number
$\underline{v_i}$	Lower limit of voltage at bus i
B_{eq}	Susceptance of VSC in an aggregated norm
E_m^{φ}	Open circuit voltage of BESS
G_{sw}	A conductance with a degree of power behavior
M	Number of tap positions
R_{int}	Internal resistance of a BESS
r_{min}/r_{max}	Minimum/maximum ratio
R_{sw}	The reciprocal of G_{sw}
$S_{VSC,i}$	Capacity of VSC
SOC_{max}	Maximum state of charge
SOC_{min}	Minimum state of charge
V_0^{ref}	Voltage vector at the source bus
v_0^{ref}	Second-order decision variable at source bus
W_{δ}	Weight coefficient for PSD
$W_{\alpha}/W_{\beta}/W_{\gamma}$	Weight coefficient for each factor
y_j	Shunt capacitance of bus j
z_{ij}	Branch resistance from bus i to bus j
C	Mechanical switching cost

Variables

R_m	Discrete tap ratio at tap m
$\mu^{\varphi}_{\mathrm{PY},i,n,t}$	Binary variable indicating PSD status of user n in bus i at time t
ξ	Slack variable of subproblem
b_i^{φ}	Binary variables used to represent tap positions
e	Continuous variables of the SP
$I_{bat}^{\varphi}/I_{sop}$	Current of BESS/SOP of phase φ
$l_{ij,t}$	Current from bus i to bus j at time t
m_a	VSC's amplitude modulation index
$P_{\mathrm{D},i,n,t}$	Active power demand of user n in bus i at time t
$P^{\varphi}_{\mathrm{D},i,t}$	Active power injection of phase φ in bus i at time t
$P^{\varphi}_{BESS,i,t}$	BESS charging power or discharging power of phase φ at bus i at time t
$P^{charge,\varphi}_{BESS,i,t}$	BESS charging power limit at bus i at time t
$P^{discharge,\varphi}_{BESS,i,t}$	BESS discharging power limit at bus i at time t
$P^{\varphi}_{VSC,i,t}$	VSC's active power of phase φ of bus i at time t
$P^{\varphi}_{VSC,Loss,i,t}$	VSC's active power loss of phase φ of bus i at time t
$Q^{\varphi}_{\mathrm{D},i,t}$	Reactive power injection of phase φ in bus i at time t
$Q_{\mathrm{D},i,n,t}$	Reactive power demand of user n in bus i at

Manuscript received: October 8, 2024; revised: February 3, 2024; acepted: April 14, 2025. Date of CrossCheck: April 14, 2025. Date of online publication: XX XX, XXXX.

This work is supported by Science and Technology Project of State Grid Corporation of China (5400-202455203A-1-1-ZN).(Corresponding authors: Wei Tang, e-mail:wei_tang@cau.edu.cn).

Chengwei Lou, Ran Zhao, Hangxing Zhang, Lu Zhang and Wei Tang (CA) are with College of Information and Electrical Engineering, China Agricultural University, Beijing, 100083, China (e-mail: chengwei.lou@cau.edu.cn; sy20233081956@cau.edu.cn; 18339797961@163.com; zhanglul@cau.edu.cn; wei_tang@cau.edu.cn). Jin Yang is with the James Watt School of Engineering, University of Glasgow, Glasgow, G12 8QQ, UK (e-mail: Jin.Yang@glasgow.ac.uk). Linjuan Zhang is with the State Grid HeNan Economic Research Institute, Zhengzhou, 450000, China (e-mail: zlinj@163.com).

DOI: 10.35833/MPCE.2024.001114

	time t
Q^{φ}_{BESS}	Reactive power of BESS of phase φ
$Q^{\varphi}_{VSC,i,t}$	VSC's reactive power of phase φ of bus i at time t
r^{φ}_{i}	Tap ratio of a transformer
s_j	Power injection at bus j
$S_{BESS,i,t}$	Energy storage present state at bus i
$S_{ij,t}$	Power from bus i to bus j at time t
V_{cap}	Voltage of a capacitor in SOP
$V_{i,t}$	Voltage vector at bus i at time t
$v_{j,t}$	Voltage at bus j at time t
W	Matrix with R^2_m as elements
w	Mixed-integer variables of the MP
Indices and sets	
$\mathcal{N}$	Set of all buses
$\mathcal{N}^+$	Set of buses without substation
$\mathcal{N}_{SOP}$	Set of all buses with SOPs
ϕ	Set of all buses with PSD
ϕ_{PY_i}, ϕ_{PN_i}	Set of single-phase users with/without PSDs
Ω_b	Set of all network branches
H	Hermitian transpose
abc	Phase components

I. Introduction

Distribution networks (DNs) span vast geographical areas, leading to an inherent three-phase imbalance [1]. The current evolution in energy consumption trends has spurred a marked proliferation of single-phase domestic electric vehicle (EV) charging stations [2] and single-phase photovoltaic (PV) power systems within these distribution networks [3].Uneven distribution of these loads among feeders leads to three-phase voltage and current imbalances in DNs. This imbalance can degrade power quality, increase power losses, and potentially damage electrical appliances. Voltage imbalances, in particular, have a pronounced impact on the performance of induction motors, causing excessively high winding temperatures that accelerate insulation material degradation and significantly reduce the machine's lifespan [4]. Furthermore, current imbalances contribute to higher distribution line losses and generate additional harmonic currents, further compromising power quality [5]. To address the imbalance in active distribution networks(ADNs) exacerbated by these developments, four existing domains have been identified: 1) Phase Configuration Adjustment, 2) Phase Switch Devices, 3) Power Electronic Device Utilization, and 4) Soft Open Point Applications.

In the **Phase Configuration Adjustment** domain, the emphasis is on static approaches. Both [6] and [7] delve into data-driven phase identification in low-voltage systems, utilizing different clustering techniques, while Homaee et al. [8] explore optimal re-phasing of single-phase customers via a discrete genetic algorithm, analyzing its effects on power losses and voltage profiles. On the other hand, Zeng et al. [9] propose a joint optimization model, incorporating Y-connected and Δ-connected static reactive power compensation devices for network balancing. However, there remains a need for further research to develop more adaptable optimization strategies that can respond effectively to the evolving demands of ADNs.

Phase Switch Devices (PSDs) offer a dynamic solution to network load balancing by allocating single-phase consumers to specific phases. Studies reveal that under constrained data and communication, the correlation between voltage unbalance sensitivity and power injection aids local control strategies for PSDs at discrete buses [10]–[12]. Addressing unbalance issues aggravated by PV generation, a study proposed an iteration-based algorithm to optimize phase connections, tackling the mixed-integer non-convex programming (MINCP) problem [13]. Another exploration emphasized the cost and efficiency advantages of automatic re-phasing over manual methods in smart distribution networks, introducing an optimal balancing method via the modified shuffled frog leaping algorithm (MSFLA) [14]. Despite prior validation, the algorithms employed the modest validation systems, potentially inadequate for delivering optimal solutions as system dimension and complexity increase. The incorporation of integer variables further complicates the resolution, necessitating a more efficient algorithm.

Power Electronic Devices in distribution networks facilitate dynamic balancing. Static Var Compensators (SVCs) redistribute current among phases as discussed in [15], while Step Voltage Regulators (SVRs) control voltage magnitude to mitigate voltage unbalance and minimize losses as seen in [16] and [17]. Distributed Generators (DGs) adjust power injection for voltage balance, with [18] exploring the three-phase adjustment ability of DG inverters. [19] and [20] focus on PV systems for local voltage balancing and coordinated multi-microgrid approaches. Lastly, [21] and [22] delve into per-phase control of three-phase DG inverters and DG aggregation to enhance network performance and flexibility. Regardless of their capability to balance the network, they are generally preset and lack the agility for inter-phase power transfer.

Soft Open Points (SOPs) provide advanced balancing in ADNs, distinguishing them from conventional devices like SVCs and PV inverters [23]. SOPs link different buses via a shared direct current link, enabling active power transfer beyond conventional power flow constraints [13], which aids DG integration and network balancing. Research [24], [25] introduced a multi-objective operational model to evaluate SOPs' balancing efficacy. Further studies [24], [26], [27] highlighted SOPs' role in mitigating voltage violations and uncertainties from PV outputs in ADNs. Phase-changing SOPs (PC-SOPs) [28], [29] and a coordination strategy employing phase-switching soft open points (PS-SOPs) and PSDs [30] were introduced for superior network balancing. Both PS-SOP and PC-SOP possess the capability for phase switching, but the former achieves real-time cross-phase power transfer through PSDs, offering higher flexibility. Additionally, [31] pioneered a phase transfer technique in MATLAB's Simulink for redistributing single-phase power across multiple phases, showcasing a novel approach to phase power management.

The aforementioned methods represent the commonly utilized infrastructures in power grids. Based on their practical performance, phase-switching devices provide an effective solution and remain a significant focus despite limitations in manufacturing and control algorithms. Capacitor-based devices are restricted to discrete adjustments and lack real-time responsiveness, whereas power-electronic-based devices

enable continuous regulation with rapid response, delivering superior performance in mitigating three-phase imbalance.

In summary, SOP, as an emerging electronic component, exerts a considerable impact on mitigating imbalances within ADNs, therefore SOP and its interaction with other components like PSD are mainly discussed in this paper. The **Research Gap** in existing models of SOPs lies in their tendency to simplify the intertwined constraints between active power and reactive power [32], making the unrealistic assumption that they can be generated independently. Contrarily, the active-reactive power dispatch model recognizes the AC power flow constraints inherent in SOPs. As outlined in [32], the votage source converter based battery energy storage system (VSC-based BESS) provides insight into the interplay between the PWM control output voltage of VSCs and BESS output power. This understanding expanded with the advent of VSC-based Energy Routers [33]. However, while AC models of SOPs consider reactive power, they fall short in exploiting the full potential of DC components, particularly in synchronizing renewable generation across distinct DC buses using individual VSC operations, impeding effective renewable energy integration into three-phase systems. Introducing PSDs adds complexity due to the emergence of integer variables. Their discrete nature complicates switching operations, thus necessitating advanced algorithmic solutions. This study outlines the challenges ADNs face from emerging single-phase loads, reviews current mitigation strategies, pinpoints research gaps, and introduces advanced control techniques.

The primary contributions of this study are as follows:

- **Component Incorporation**: Compared with the foundational SOP model, this work introduces a integration of PWM technology with the VSC component, leading to a three-phase VSC-driven modelling approach for SOP. This integration enhances model accuracy by detailing the interplay between the PWM control output voltage of VSCs and power output, encapsulating the explicit circuit relationship among them for refined regulation, and considering utility voltage changes for further power regulation refinement. Placement of these components in buses with notable power imbalances enhances system efficiency, showcasing the benefits of the integrated approach.
- **Performance Improvement**: The paper presents an innovative fusion of three-phase VSC-driven modelled SOPs and BESS, harmoniously operating alongside PSDs. This synergistic approach effectively mitigates power losses throughout the distribution network. Meanwhile, it significantly enhances the system's three-phase balance. The resulting model demonstrates both heightened efficiency and eminent potential for deployment in practical electrical network settings.
- **Optimization Algorithm**: The paper unfolds a systematic optimization for balancing three-phase electrical systems, incorporating PSDs, BESS, and SOP. Beginning with crucial system parameters and BESS/SOP placements, it advances through three-phase VSC-driven model constructions. The strategy leverages symmetrical semidefinite programming (SDP) algorithms, introducing convex relaxation and forming a mixed-integer SDP (MISDP). Moreover, this study formulates an efficacious algorithm predicated on Benders decomposition (BD), augmented with a Bound-tightening strategy, to address the solution of the problem.

The paper is organized as follows: Section II details the optimal coordination model, which begins by elucidating the theoretical underpinnings, encompassing the principles of VSC and PWM technologies, and subsequently introduces the control relationship between that and model parameters. Section III proceeds to showcase case studies involving various scenarios, facilitating comparisons and result analysis aimed at validating and evaluating the proposed model's superiority in power transmission and mitigating network losses. Finally, Section IV concludes the paper.

II. Methodology

The overarching architecture of the analyzed system is depicted in Fig 1.(a). Models of three-phase VSC-driven BESSs and three-phase VSC-driven SOPs are showcased in Fig 1.(b) and Fig 1.(c), respectively. There are three mechanisms to enhance power provision optimization: BESS, which is harnessed for energy containment and dispatch; PSD, which is deployed for adept load orchestration; and PV, elucidating the impacts of DG. Model preliminaries are provided in Supplementary Material.I.

A. Optimal Power flow of three-phase AC DNs

For each line segment from bus i to bus j, the bus voltage vectors are defined as V_i and V_j, and the current I_{ij}. The second-order decision variables are $v_i = V_i V_i^H$, $l_{ij} = I_{ij} I_{ij}^H$, and $S_{ij} = V_i I_{ij}^H$.

The symmetrical SDP model is employed due to the superior numerical precision compared with the traditional model [34]. Index the substation bus by 0 and other buses by 1, 2, …, n. Let $\mathcal{N}$ denote the set of all buses and $\mathcal{N}^+ = \mathcal{N} \setminus \{0\}$. Voltages in phase components are transformed into symmetrical components as follows [35]:

$$V_{i,t}^{abc} = A V_{i,t}^{012} \tag{1}$$

$$A = \frac{1}{\sqrt{3}} \begin{bmatrix} 1 & 1 & 1 \\ 1 & a^2 & a \\ 1 & a & a^2 \end{bmatrix} \tag{2}$$

where $a = 1\angle 120^\circ$ and $A^H = A^{-1}$. Consequently, the three-phase variables and the impedance parameters are correlated with the equivalent variables in symmetrical components:

$$\begin{cases} v_{i,t}^{abc} = V_{i,t}^{abc} \cdot V_{i,t}^{abc,H} = A V_{i,t}^{012} \cdot (A V_{i,t}^{012})^H = A v_{i,t}^{012} A^H \\ l_{ij,t}^{abc} = A l_{ij,t}^{012} A^H \\ S_{ij,t}^{abc} = A S_{ij,t}^{012} A^H \\ z_{ij,t}^{abc} = A z_{ij,t}^{012} A^{-1} = A z_{ij,t}^{012} A^H \\ y_{i,t}^{abc} = A y_{i,t}^{012} A^{-1} = A y_{i,t}^{012} A^H \end{cases} \tag{3}$$

The structure of the branch impedance matrix in the sequence system is related to the self-impedances and mutual impedances of the branches in the phase system. As stated

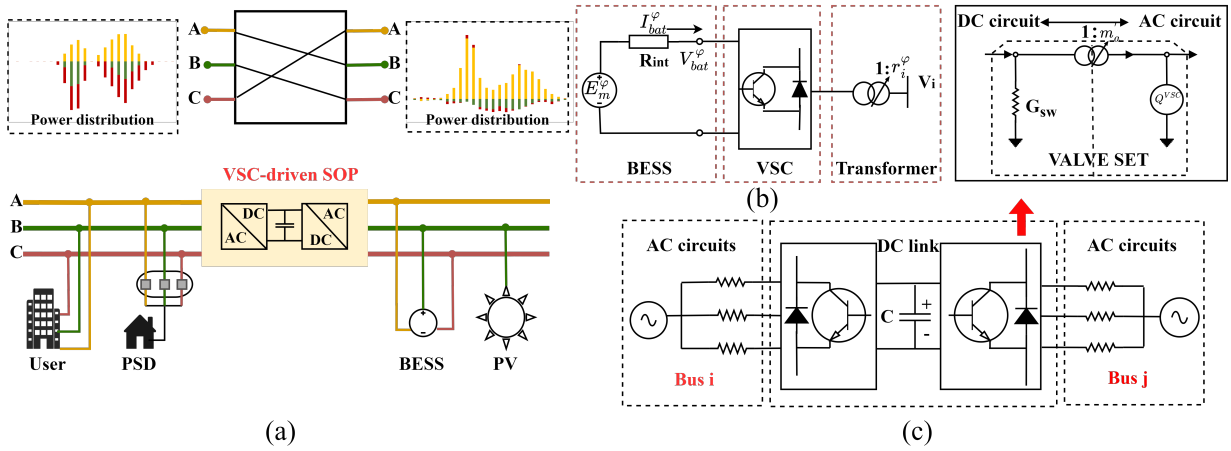

Fig. 1. (a) Architecture of the analyzed distribution system (b) BESS equivalent circuit (c) Three-phase VSC-driven SOP equivalent circuit

in 'Analysis of Faulted Power Systems' [36], in most computations, it is assumed that the self-impedances and mutual impedances are equal within each phase and between phases, respectively, to decouple the sequences, thus obtaining the diagonalized matrix.

Consequently, power flow balance constraint at time t is:

$$\begin{aligned}&\sum_{ij\in\Omega_b} diag(A(S_{ij,t}^{012}-z_{ij}^{012}l_{ij,t}^{012})A^H)\\&+s_{j,t}+y_{j,t}^{012}v_{j,t}^{012}=\sum_{jk\in\Omega_b} diag(AS_{jk,t}^{012}A^H)\end{aligned} \tag{4}$$

Kirchoff's voltage law along line ij at time t:

$$v_{j,t}^{012}=v_{i,t}^{012}-(S_{ij,t}^{012}z_{ij}^{012,H}+S_{ij,t}^{012,H}z_{ij}^{012})+z_{ij}^{012}l_{ij,t}^{012}z_{ij}^{012,H} \tag{5}$$

Equation (6) imposes the lower and upper limits on the voltage of bus i at time t, whereas Equation (7) defines the voltage at the source bus. Equation (8) expresses the positive semidefinite constraint.

$$\underline{v_{i,t}}\le diag(Av_{i,t}^{012}A^H)\le\overline{v_{i,t}}\ ,i\in\mathcal{N} \tag{6}$$

$$v_0^{012}=V_0^{012,ref}(V_0^{012,ref})^H \tag{7}$$

$$\begin{bmatrix}v_i^{012} & S_{ij}^{012}\\ S_{ij}^{012,H} & l_{ij}^{012}\end{bmatrix}\succeq 0\ ,i\to j \tag{8}$$

Single-phase and two-phase branches are modeled as equivalent three-phase lines, with dummy lines and buses preserving the three-phase structure [37], enabling their representation in sequence networks. The series impedances of the dummy lines can be set to arbitrary values. Therefore, the conversion of symmetrical component variables back to phase variables is applied for those buses connected to single-phase or two-phase branches [34].

Finally, the symmetrical SDP model is subject to constraints (9)–(13) for single-phase and two-phase branches, and constraints (4)–(8) for the three-phase backbones.

$$\sum_{ij\in\Omega_b} diag(S_{ij,t}-z_{ij}l_{ij,t})+s_{j,t}+y_{j,t}v_{j,t}=\sum_{jk\in\Omega_b} diag(S_{jk,t}) \tag{9}$$

$$v_{j,t}=v_{i,t}-(S_{ij,t}z_{ij}^H+S_{ij,t}^Hz_{ij})+z_{ij}l_{ij,t}z_{ij}^H \tag{10}$$

$$\underline{v_{i,t}}\le diag(v_{i,t})\le\overline{v_{i,t}}\ ,i\in\mathcal{N} \tag{11}$$

$$v_0=V_0^{ref}(V_0^{ref})^H \tag{12}$$

$$\begin{bmatrix}v_{i,t} & S_{ij,t}\\ S_{ij,t}^H & l_{ij,t}\end{bmatrix}\succeq 0\ ,i\to j \tag{13}$$

B. Modelling of three-phase VSC-driven SOP

In the modelling depicted in Fig. 1 (a), we introduce a three-phase VSC-driven SOP comprising an AC/DC VSC, a DC capacitor, and a DC/AC VSC. The equivalent representation of an VSC is elucidated in Fig. 1 (c). As modeled in Fig. 1, the operation of the VSC can be analogized to an ideal complex tap-changing transformer, a concept derived from [33].

The foundational relationship inherent to the PWM controlled operation of VSCs:

$$\begin{aligned}|V_i^\varphi|&\le m_a'|V_{cap}|\\|V_j^\varphi|&\le m_a'|V_{cap}|\end{aligned} \tag{14}$$

The VSC adheres to the relation m_a' as outlined in [32]. Furthermore, the switching losses of the converter can be quantified as [32]:

$$P_{VSC,Loss}^\varphi=G_{sw}V_{cap}^2 \tag{15}$$

The VSC is approximated by a combination of a resistor and a reactive power source, as illustrated in Fig. 1(c). The resistor's incorporation ensures connectivity to the grid's resistive component. Concurrently, the reactive power source exclusively delivers reactive power to the AC converter buses, thereby improving the reactive compensation capability.

The operation of the three-phase VSC-driven SOP is constrained by capacity limitation and power losses, which can be described as follows:

$$|||[P_{VSC,i,t}^\varphi,Q_{VSC,i,t}^\varphi]|||_2\le S_{VSC,i} \tag{16}$$

$$\begin{aligned}&\sum_\varphi(P_{VSC,i,t}^\varphi+P_{VSC,Loss,i,t}^\varphi)+\\&\sum_\varphi(P_{VSC,j,t}^\varphi+P_{VSC,Loss,j,t}^\varphi)=0\end{aligned} \tag{17}$$

C. Modelling of three-phase VSC-driven BESS

The three-phase BESS model is adopted, yet the power can be managed separately by phase. The simplified circuits of the individual phase of VSC-driven BESS model are shown in Fig. 1 (b), including three essential elements: a VSC, a battery and a transformer [38]. The internal circuit of the battery adheres to the equation that $V_{bat}^{\varphi} = E_m^{\varphi} - I_{bat}^{\varphi} R_{int}$, and V_{bat}^{φ} is approximated to E_m^{φ} [32], making internal losses not factored into the constraints but optimized in the objective function. Therefore, the power flow and output voltage satisfy the following equations:

$$\begin{cases} P_{BESS}^{\varphi} = E_m^{\varphi} I_{bat}^{\varphi} \\ Q_{BESS}^{\varphi} = m_a'^2 B_{eq} E_m^{\varphi 2} \\ |V_i^{\varphi}| = m_a' \cdot r_i^{\varphi} \cdot E_m^{\varphi} \end{cases} \tag{18}$$

Specifically, r_i^{φ} is modeled as in Equation (19) with binary variables [39].

The sum of $b_{i,m}^{\varphi}$ to 1 yields a single ratio.

$$r_i^{\varphi} = \sum_{m=0}^{M} \underbrace{(r_{min} + \Delta r_i^{\varphi} \times m)}_{R_m} b_{i,m}^{\varphi} \tag{19}$$

$$\sum_{m=0}^{M} b_{i,m}^{\varphi} = 1, \quad b_{i,m}^{\varphi} \in \{0,1\} \tag{20}$$

Because $\sum_{m=0}^{M} b_{i,m}^{\varphi} = 1$ and there is only one $b_{i,m}^{\varphi}$ being 1 with the rest being 0, also $(b_{i,m}^{\varphi})^2 = b_{i,m}^{\varphi}$, then $r_i^{\varphi 2} = \sum_{m=0}^{M} R_m^2 b_{i,m}^{\varphi} = W \cdot b_i^{\varphi}$.

Equation (18) is non-convex due to the product between a continuous and a discrete variable for $|V_i^{\varphi}|$. Following the variables' alteration, it can be reformulated as

$$\begin{aligned} v_i^{\varphi} &= V_i^{\varphi 2} = m_a'^2 r_i^{\varphi 2} \cdot E_m^{\varphi 2} \\ &= x_i \cdot r_i^{\varphi 2} \cdot E_m^{\varphi 2} = W \cdot E_m^{\varphi 2} \cdot (x_i \cdot b_i^{\varphi}) \end{aligned} \tag{21}$$

The nonlinear product $x_i \cdot b_i^{\varphi}$ is represented by $T_{i,m}$:

$$T_{i,m} = x_i \cdot b_i^{\varphi}, i \in \mathcal{N}_B \tag{22}$$

According to [32], Equation (22) can be replaced by the following constraints to solve:

$$\underline{x}_i \cdot b_i^{\varphi} \le T_{i,m} \le \overline{x}_i \cdot b_i^{\varphi} \tag{23}$$

$$\underline{x}_i (1 - b_i^{\varphi}) \le x_i - T_{i,m} \le \overline{x}_i (1 - b_i^{\varphi}) \tag{24}$$

BESS operation constraints are as follows:

$$\begin{cases} S_{BESS,i,t} = S_{BESS,i,t-1} + \sum_{\varphi} P_{BESS,i,t}^{\varphi} \\ |P_{BESS,i,t}^{charge,\varphi}| \le |P_{BESS,i,t}^{\varphi}| \le |P_{BESS,i,t}^{discharge,\varphi}| \\ SOC_{\min} \le S_{BESS,i,t} \cdot S_{rated,i}^{-1} \le SOC_{\max} \end{cases} \tag{25}$$

The power loss of three-phase VSC-driven BESS follows Eq (15).

D. Integration of PSD

For a specific bus, designated as i, consumers can be delineated into two categories: those equipped with a PSD, represented by ϕ_{PY_i}, and those devoid of such a device, symbolized as ϕ_{PN_i}, $\phi_{PY_i} \cup \phi_{PN_i} = \phi$. The latter subset is further stratified based on their connected phase into $\phi_{PN_i^a}, \phi_{PN_i^b}$, and $\phi_{PN_i^c}$. Consequently, the power injection for a bus equipped with a PSD can be articulated as [30]:

$$\begin{aligned} & P_{\mathrm{D},i,t}^{\varphi} + \mathbf{i} Q_{\mathrm{D},i,t}^{\varphi} = \sum_{n \in \phi_{PN_i}^{\varphi}} \left(\bar{P}_{\mathrm{D,i,n,t}} + \mathbf{i} \bar{Q}_{\mathrm{D},i,n,t} \right) \\ & + \sum_{n \in \phi_{\mathrm{PY_i}}} \mu_{\mathrm{PY_i},i,n,t}^{\varphi} \left(\bar{P}_{\mathrm{D},i,n,t} + \mathbf{i} \bar{Q}_{\mathrm{D},i,n,t} \right), \\ & \sum_{\varphi} \mu_{\mathrm{PY_i},i,n,t}^{\varphi} = 1, i \in \phi, n \in \phi_{\mathrm{PY_i}}, \forall t \\ & \mu_{\mathrm{PY_i},i,n,t}^{\varphi} \in \{0,1\}, i \in \phi, n \in \phi_{\mathrm{PY_i}}, \forall t \end{aligned} \tag{26}$$

E. Overall Optimization Problem Using BD

Continuous and binary variables are denoted as $e = \{v, S, \ell\} \in \mathcal{E}$ and $w = \{r, T, b, \mu\} \in \mathcal{W}$, respectively.

Network loss function is:

$$F(e) = W_\alpha \times F_1 + W_\beta \times F_2 + W_\gamma \times F_3 \tag{27}$$

The calculation formulas for the losses of line, SOP, and BESS are presented in sequence as follows:

$$F_1 = sum(P_D + P_{BESS} + P_{PV} - P_{LOAD}) \tag{28}$$

$$F_2 = I_{sop}^2 (R_{sw} + R_{int}) \tag{29}$$

$$F_3 = I_{bat}^2 (R_{sw} + R_{int}) \tag{30}$$

Solving MISDP directly is particularly complex due to the inclusion of integer decision variables, often resulting in computational infeasibility. This issue can be effectively managed through Benders decomposition (BD) [40], where the original problem is partitioned into a mixed-integer linear programming master problem and an SDP subproblem, solved iteratively. It helps overcome issues of local optimality caused by integer decision variables, ensuring the convergence of algorithm [41]. Furthermore, the iterative process, which gradually approaches the optimal solution, significantly enhances computational efficiency [42]. Therefore, BD is applied in this paper to decouple and solve the origin problem effectively. Master problem and subproblem are written as MP and SP respectively. In each iteration, the binary variable solution from the MP is passed to the SP, and the solution of the SP generates an optimality cut for the MP.

Besides, a bound-tightening (BT) strategy is employed to solve the ratio bounds faster [39]. The outcome serves as one of the constraints for the MP, ensuring that the MP solution is always feasible for the SP, thereby eliminating the generation of feasible cuts.

$$\begin{aligned} & \mathbf{BT}: \min(\text{or } \max) \sum_{i \in N^+} \sum_{\varphi} v_i^{\varphi} \\ & \text{s.t. } \underline{x}_i \cdot E_m^{\varphi 2} \le v_i^{\varphi} \le \overline{x}_i \cdot E_m^{\varphi 2}, \quad \forall \varphi, i \in \mathcal{N}^+ \\ & (4), (5), (6), (7), (8) \end{aligned} \tag{31}$$

Ratio bounds are computed as $\underline{R_i}(\overline{R_i}) = v_i^{\varphi}/(x_i \cdot E_m^{\varphi 2})$.

Considering the cost associated with mechanical switching [40], MP is formulated as below:

$$\begin{aligned} &\textbf{MP}: \theta_{lb} = \min \eta + C \cdot w \\ &\text{s.t. } \eta \geq F(e^*) + \sum_{i \in N^+} \sum_{\varphi} \lambda^{\varphi,k} W^{'}(w_i^{\varphi} - w_i^{\varphi,k}), k = 1, 2, \dots \\ &\underline{R_i} \leq W \cdot b_i^{\varphi} \leq \overline{R_i}, \forall \varphi, i \in \mathcal{N}^+ \\ &(19), (20), (23), (24), (26), \quad w \in \mathcal{W} \end{aligned} \tag{32}$$

The superscript (*) distinguishes quantities obtained from the SP, and $W^{'} = \begin{bmatrix} W \\ W_{\delta} \end{bmatrix}$. Relative to the line losses, the costs attributed to the modulation of VSC and PSD are marginal and can be neglected. The optimal objective of MP provides the lower bound (θ_{lb}). The solution of MP $\hat{w}$ is guaranteed to be feasible for SP upon solving the BT. As for SP, a slack variable ξ is added to return optimality cuts, where $\sigma \gg 0$ [43].

$$\begin{aligned} &\textbf{SP}: \theta_{ub} = \min F(e) + \sigma \cdot \xi \\ &\text{s.t.} \quad \xi \geq 0, \\ &(4)\text{–}(13), (21), (25), (21), (23), \quad e \in \mathcal{E}, \quad \hat{w} \in \mathcal{W} \end{aligned} \tag{33}$$

If SP has a solution for b_i^{φ} obtained from the MP, the optimal objective to SP is an upper bound (θ_{ub}) to the original problem. It also provides optimal Lagrangian multipliers $\lambda^{\varphi,k}$ associated with the binary variables to create optimality cuts that constrain the MP, where k denotes the iteration. The optimality of the solution is measured by the gap between θ_{lb} and θ_{ub}. The problems iterate until the pre-defined tolerance ϵ for the gap is met, thus achieving the optimal solution [44].

The whole operational optimization process is depicted in **Algorithm 1**, which delineates a systematic approach for optimizing a three-phase distribution network. Firstly, the basic parameters of the network are input, and component modeling is carried out. By leveraging symmetrical SDP method, convex relaxation techniques are applied, followed by a three-phase decoupling . Benders decomposition scheme is applied to solve the MISDP problem. The algorithm then verifies the necessity of PSD optimization. If required, reformulation of MP is embarked upon. The derived optimal result also undergoes a convergence check. Finally, the process either concludes or revisits the optimization step.

Algorithm 1 Optimization Algorithm for MISDP Problem

1: **Start**
2: **Initialization:**
    Input initial three-phase parameters
    Specify locations of BESS and SOP
3: **Model Setup:**
    Construct three-phase VSC-driven SOP/BESS model
    Define objective function and constraints
4: Use symmetrical SDP method to perform three-phase decoupling
5: **Apply Benders decomposition:**
6: Pick any $b_i^{\varphi} \in \mathcal{W}$. Initialize $\theta_{lb}^0 = -\infty$ and $\theta_{ub}^0 = \infty$
7: Solve BT to obtain $\underline{R_i}$ and $\overline{R_i}$
8: **while** $\epsilon \leq |\theta_{ub}^k - \theta_{lb}^k|$ **do**
    Solve MP($\underline{R_i}$, $\overline{R_i}$), update θ_{lb}^k and $\hat{w}$
    Solve SP, update θ_{ub}^k and generate optimality cuts
    Increase k by 1
9: **end while**
10: Initialize phase setting of PSD
11: **if** PSD optimization is not required **then**
12: **Terminate Algorithm**
13: **end if**
14: **PSD Optimization:**
    Formulate the new MP by updating W_{δ} from initial **0** and adding constraint (26)
    Obtain the action decisions
15: **if** $|\theta_{ub}^k - \theta_{lb}^k| < \epsilon$ **then**
16: **Terminate Algorithm**
17: **else**
    Update output of SOP, BESS and PSD
    Return to Step 7 for re-optimization
18: **end if**

F. The Practical Challenges of SOP

While the application of SOPs enhances ADNs' operation and reduces power losses, the cost implications of deploying such devices warrant further investigation [45]. To evaluate the economic feasibility of the proposed approach, the reduction in power loss costs is compared with the implementation costs, which include both investment and operational expenses. The method is deemed feasible if the former equals or exceeds the latter [46]. Cost formulas and relevant parameters are based on [47] and are detailed in Supplementary Material.II.

III. CASE STUDY

According to the study [29], the evaluation of the three-phase VSC-driven SOP was carried out using an adapted IEEE 123-bus distribution network in this research, as illustrated in Fig. 2 (a). The network incorporates ten strategically positioned PV systems across varied buses. Specifically, SOP1 is connected between buses 151 and 300 with a capacity of 150 kVA, whereas SOP2 establishes a connection between buses 54 and 93 with a capacity of 300 kVA. And BESS has a cumulative capacity of 1.50 MVA. The modellings employed encompass $B_{\text{eq}} = 0.001S$, $R_{\text{sw}} = 0.2$ p.u., $R_{\text{int}} = 0.44$ p.u., and $E_m = \sqrt{2}V_{\text{base}}$, where V_{base} denotes the system's base voltage. Three-phase active power of load is depicted in Fig. 2 (b), where the reactive power trend aligns with it. The PV generation profile is consistent with the patterns shown in Fig. 2 (c). Voltage regulators are tuned as follows: for buses 150 to 149 (three-phase), $[r_t^a \ r_t^b \ r_t^c]$=[1.04375 1.04375 1.04375] , for buses 9 to 14 (single-phase) r_t^a=0.99375 , for buses 25 to 26 (two-phase) $[r_t^a \ r_t^c]$=[1 0.99375] , and for buses 67 to 160 (two-phase) $[r_t^a \ r_t^b \ r_t^c]$=[1.05 1.00625 1.03125] . The voltage constraints for all buses are set as [0.94, 1.10]. The symmetric SDP approach proposed is implemented using the YALMIP toolbox [48] and optimized by the MOSEK solver. The 34-bus validation case is documented in Supplementary Material.III.

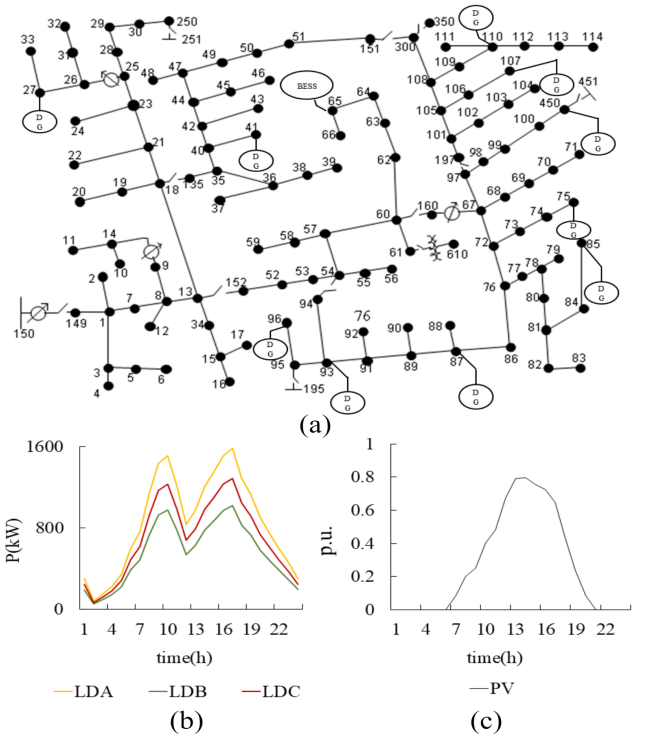

Fig. 2. (a) Test network with IEEE 123-bus topology (b) Three-phase active power of load (c) PV output profile

TABLE I
COMPARATIVE ANALYSIS OF TRADITIONAL VS. THREE-PHASE VSC-DRIVEN SOP PERFORMANCE METRICS

	case A		case B	
	SOP1	SOP2	SOP1	SOP2
Line Loss (MW(24h))	0.7382		0.7302	
Imbalance Index (1E-2)	8.58		7.07	
SOP Active Power (kW(24h))	113.91	396.89	302.72	1375.38
SOP Reactive Power (kVar(24h))	352.26	234.97	890.31	484.24
SOP Losses (kW(24h))	8.73	17.28	12.21	32.84

A. Comparative Analysis of Traditional and three-phase VSC-driven SOP Modellings

In the traditional SOP model, the fixed loss coefficient for an SOP is assumed to be $\gamma^{VSC} = 0.02$ as proposed in [49]. The loss for the SOP is represented by the equation:

$$P^{\varphi}_{VSC,Loss,i,t} = \gamma^{VSC}\sqrt{(P^{\varphi}_{VSC,Loss,i,t})^2 + (Q^{\varphi}_{VSC,Loss,i,t})^2} \quad (34)$$

To highlight the merits of the three-phase VSC-driven SOP model, two representative cases are presented, with their details provided as follows. BESS with charging/discharging mode is adopted within the comparison. Therefore case B in this section is same as case 2 in the following section B.

case A: Traditional SOP interfacing buses 151-300 (SOP1) and buses 54-93 (SOP2) [49].

case B: Three-phase VSC-driven SOP connecting buses 151-300 (SOP1) and buses 54-93 (SOP2).

TABLE I delineates the comparative metrics between the traditional SOP (case A) and the three-phase VSC-driven SOP (case B) for both SOP1 and SOP2, several critical insights emerge. Notably, losses and power output are derived as the sum over a 24-hour period, and SOP's active power is the sum of the power transmitted among phases. Firstly, there's a clear reduction in line loss when transitioning from case A (0.7382 MW) to case B (0.7302 MW), suggesting an enhanced efficiency with the three-phase VSC-driven SOP. Moreover, the three-phase VSC-driven SOP in case B notably boosts active power transmission, especially for SOP2, which shows an increment of 978.49 kW relative to case A. The loss percentage in case B, defined as the ratio of SOP losses to SOP active power, stands at a more efficient 2.39% for SOP2, as opposed to the 4.35% in case A. Additionally, case B's SOP1 presents a significant increase in reactive power supply, with values at 890.31 kVar compared to 352.26 kVar in case A. Another crucial metric is the three-phase imbalance index, which can be calculated as detailed in [29]. The three-phase VSC-driven SOP in case B evidences a decline to 7.07 x 10E-2 from the 8.58 x 10E-2 in case A, highlighting its ability to better balance the system. In summary, the data in TABLE I advocates for the superior efficiency and operational benefits of the three-phase VSC-driven SOP (case B) over the traditional approach, especially when considering

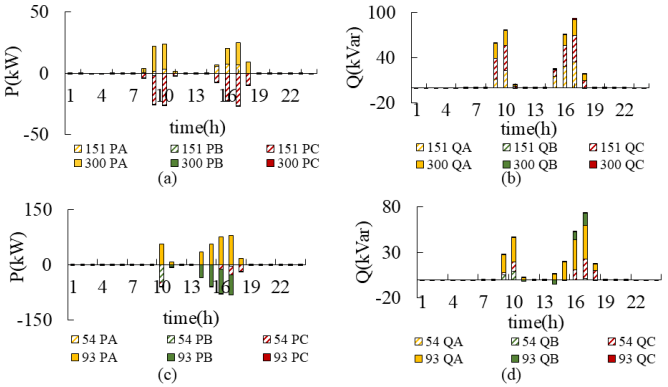

Fig. 3. Three-phase power generation of traditional model-(a) active power of SOP1 (b) reactive power of SOP1 (c) active power of SOP2 (d) reactive power of SOP2

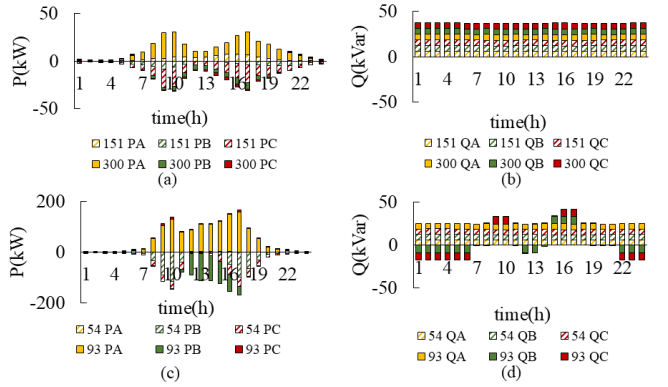

Fig. 4. Three-phase power generation of proposed model-(a) active power of SOP1 (b) reactive power of SOP1 (c) active power of SOP2 (d) reactive power of SOP2

the cumulative performance of both SOP1 and SOP2.

Fig. 3 and Fig. 4 clearly illustrate the power generation of the traditional and proposed model, respectively. In the context of SOP1 for case A, the initial morning hours, spanning from 1 to 7, present a notably reserved active power transfer pattern. Most prominently, a peak of 0.05537 kW in Phase A is identified at the 7th hour for bus 151. However, by the 8th hour, a significant increase in power transfer dynamics is evident. By the 10th hour, this uptrend culminates with bus 300's Phase A recording a considerable active power transfer of 20.55 kW. This pronounced increase is subsequently offset by a period of relative inactivity from the 11th to 15th hours, where transfer values gravitate towards zero. The zenith of power transfer for SOP1 emerges at the 17th hour: bus 151's Phase C registers a value of -26.40 kW, while simultaneously transferring -26.40 kW to its Phase A, which measures 6.65 kW, and to bus 300's Phase A, marked at 18.28 kW. Delving into the reactive power metrics, bus 151's Phase A exhibits two noteworthy peaks: a value of 76.28 kVar at the 10th hour, and a heightened 92.07 kVar by the 17th hour. As the system progresses towards the evening hours, specifically from 19 to 24, a decline in both active and reactive power transfers is observable, with magnitudes largely confined to the 1E-05 to 1E-06 range.

In the appraisal of Scenario SOP2 for case A, the early hours, from 1 to 7, exhibit a active power transfer trend akin to SOP1. Notably, by the 7th hour, bus 151's Phase A delineates a peak that aligns with the aforementioned scenario. Progressing to the 8th hour, a marked escalation in power transfer is observable. The crescendo of this pattern is attained by the 10th hour, as bus 300's Phase A logs an active power transfer of 56.06 kW. The subsequent interval, from the 11th to 15th hours, mirrors SOP1's trend, registering near-zero transfer values. The pinnacle of power transfer for SOP2 surfaces at the 17th hour with bus 93's Phase A indicating a notable 79.64 kW. Subtle variations are discerned in the reactive power data for bus 151's Phase A, yet it maintains a similar bifurcated peak structure to SOP1. Transitioning into the dusk hours, from 19 to 24, there's an evident tapering in both active and reactive power transfers, converging mainly within the 1E-05 to 1E-06 domain.

In the context of SOP1 within case B, there is a minimal active power transmission during the early morning hours (1-5 am), amounting to a total transfer of 8.10 kW. However, between the hours of 6 to 10 am, there is a notable surge in power generation within Phase A at bus 300, attaining peak values of 27.20 kW and 26.80 kW at the 9th and 10th hours, respectively. Subsequently, during the hours of 11 to 1 pm, the power output in the C-phase experiences a marginal decline, stabilizing at 4.60 kW. Nevertheless, from 2 to 5 pm, it undergoes a resurgence, culminating in a zenith of 18.60 kW at 5 pm. Thereafter (6-12 pm), there is a gradual reduction in power, dwindling to a mere 1.20 kW. It's worth noting that the reactive power output remains relatively consistent throughout the day, with each phase consistently contributing approximately 6.00 kVar/h.

For SOP2 in case B, there is limited active power during the hours of 1-7 am. At 7 am, Phase A of bus 93 absorbs 12 kW of active power. From the 8th to the 10th hour, Phase A of bus 93 undergoes a rapid escalation in power absorption, surging from 52.60 kW at 8 am to a zenith of 130.50 kW at 10 am. Another phase of ascendant power unfolds from 11 to 5 pm, culminating in a pinnacle of 158.50 kW at 5 pm. As the clock advances to 6 pm to 12 pm, power descends gradually from 92.80 kW to a mere 0.40 kW. Regarding reactive power, both Phase B and C of bus 54, along with Phase A of bus 93, exhibit negligible fluctuations, maintaining at approximately 8.60 kVar. From 1 to 6 am, both Phase B and C of bus 93 emit 8.60 kVar of power per hour. Between 7 am and 9 pm, with the exception of Phase B emitting 8.60 kVar of power from 12 to 1 pm and from 3 to 5 pm, and Phase C emitting 8.60 kVar of power from 9 to 10 am and from 4 to 5 pm, both phases maintain a marginal magnitude of reactive power, averaging around 0.15 kVar and 0.0024 kVar, respectively. From 10 pm to 12 pm, Phase B and C emit 8.60 kVar of power.

Upon evaluating the power transfer capabilities and reactive power supplementation between case A and case B across both SOP1 and SOP2 scenarios, several distinct trends are evident. In both the SOP1 and SOP2 situations, case A presents a more reserved approach to active power transfer, particularly during the initial hours, at hour 10, and spanning from hour 14 to hour 18. In contrast, case B displays superior power transmission proficiencies, manifesting prominently in SOP1 (average 19.90 kW) and in SOP2 between hour 8 to hour 20 (average 100.03kW). Furthermore, case B offers a more uniform reactive power output, with buses consistently delivering contributions ranging from 6.00 kVar up to 8.60 kVar. This consistency underscores an enhanced voltage performance and improved reactive support in case B. Due to the crucial inclusion of a reactive power source in the proposed SOP model, the reactive power output of traditional model is passively high only at certain time zones, whereas that in the proposed model is actively high throughout the day. The traditional model's fixed loss coefficients also fall short in accurately capturing the intricate quadratic relationships of losses inherent in the three-phase VSC-driven approach. This nuance in the VSC model not only reduces power losses but also augments power transfer capabilities.

The cost analysis of SOP is shown in TABLE II. The network loss cost without SOP is calculated to investigate the economic feasibility of SOP. In case A, the operating cost coefficient of SOP is 0.015, thereby reflecting the efficiency difference in power transmission between two types of SOP.

TABLE II
ANNUAL COST OF DIFFERENT SCHEMES

	Without SOP	case A	case B
C_{INV}(\$)	/	1,415.34	1,415.34
C_{OPE} (\$)	/	2,084.40	1,389.60
C_{LOSS} (\$)	50,069.24	22,314.93	22,637.3
Total cost (\$)	50,069.24	25,814.67	25,442.24

TABLE II shows that the application of SOP in case B has best economic benefits. The annual total cost of case B is \$25,442.24, less than that of without SOP, decreased by \$24,627 (reduction of 49.14%). It also represents the value by which the reduction in power loss costs exceeds the

implementation costs. Moreover, compared with case A, the total cost of case B reduces by $372.43. Thus, the installation of SOP is demonstrated to be feasible.

B. Comparative Analysis of Traditional and three-phase VSC-driven BESS Modellings

In the traditional BESS model, the interdependence between active and reactive power outputs is neglected, as well as the relationship between the PWM-VSC control architecture and bus voltage.

Four cases are designed to show the benefits of three-phase VSC-driven BESS model. Three-phase VSC-driven SOP model is used in the comparison of BESS models.

case 1: Three-phase VSC-driven BESS with constant voltage (E_m^{φ}, DC voltage control in [23]).

case 2: Three-phase VSC-driven BESS with charging/discharging mode(P/Q control in [23]) same as case A in the last section.

case 3: Traditional BESS with constant voltage (E_m^{φ}, DC voltage control in [23]).

case 4: Traditional BESS with charging/discharging mode (P/Q control in [23]).

TABLE III
COMPARATIVE PERFORMANCE METRICS OF THREE-PHASE VSC-DRIVEN AND TRADITIONAL BESS MODELLINGS

	case 1	case 2	case 3	case 4
Line loss(MW)	0.7889	0.7302	0.7943	0.7754
Improvement Rate	0.68%	5.83%	/	/
P(MW)	0.8136	2.0000	0.4871	0.5000
Q(MVar)	0.4714	0.4732	0.0422	0.0433
Imbalance Index(1E-2)	7.22	7.07	7.27	7.01

Drawing from the data presented in TABLE III, the three-phase VSC-driven BESS model, especially with charging/discharging mode (case 2), distinctly emerges as the most proficient configuration. It not only reports the minimal line loss at 0.7302 MW(24h) but also champions a reactive power supply of 0.4732 MVar(24h). Comparatively, this charging/discharging mode, both in case 2 (three-phase VSC-driven) and case 4 (traditional), consistently outperforms the constant voltage control modellings evidently in cases 1 and 3. A systematic reduction in active power losses is also discernible, with a substantial improvement rate of 5.83% when transitioning from case 4 to case 2, and a smaller yet notable shift of 0.68% from case 3 to case 1. Addressing the three-phase imbalance, the three-phase VSC-driven BESS in cases 1 and 2 registers a slight decrease in imbalance indices at 7.22 x 10E-2 and 7.07 x 10E-2, respectively, compared to the traditional models in cases 3 and 4. The minimal index of 7.01 x 10E-2 in case 4 suggests the potential efficacy of the charging/discharging mode in traditional systems, but when juxtaposed with the high reactive power supply and efficiency benefits of the three-phase VSC-driven model in case 2, the latter's superiority is unequivocal. Cumulatively, these findings cement the proposition that three-phase VSC-driven BESS, particularly in charging/discharging modes, holds the promise of optimizing network performance in ways that traditional modellings may not fully achieve.

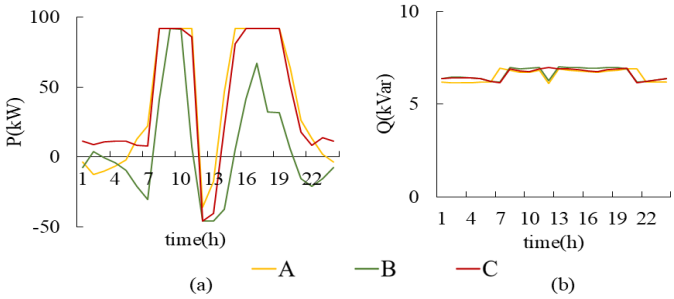

Fig. 5. (a) Three-phase active power of case 2 (b) Three-phase reactive power of case 2

As shown in the Fig. 5, the active power of the BESS in case 2 is analyzed. Combining the load curve and PV curve, it can be observed that the trend of curve variation is similar to that of the load curve, and the occurrence of peaks and valleys is related to the output of the PV source. The load curve has a peak load in the morning and afternoon, forming the peak segment. The early morning represents the load valley, forming the valley segment. From the figure, it can be seen that the BESS needs to be charged from the system in the early morning. As the load increases, the power output from the BESS gradually increases after absorbing the power from the PV source. 11 am to 3 pm is the peak period for PV, and BESS absorbs the excess active power of network. After 4 pm, BESS reaches its charging limit and enters the power generation mode. After 5 pm, the PV output power gradually decreases to zero, and BESS provides power to the load. After 9 pm, the state of charge of the BESS decreases to approximately the initial value, completing the charging and discharging process within one cycle. Here, the reactive power of BESS, like three-phase VSC-driven SOP, has been equivalently transformed into a constant source, providing stable power.

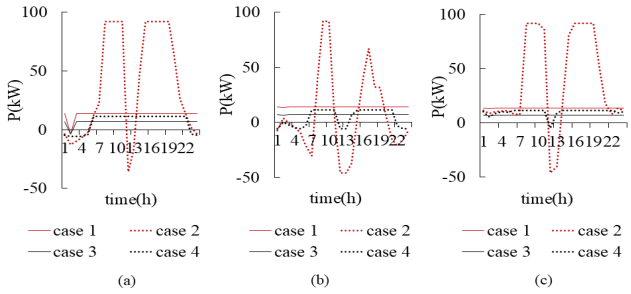

Fig. 6. Active power of BESS in four cases -(a) phase A (b) phase B (c) phase C

Fig. 6 and Fig. 7 clearly show the comparison of active and reactive power for mentioned four scenarios. Derived from the graphs displayed in Fig. 6, it becomes evident that in the context of charging/discharging mode, the novel model exhibits a significantly expanded active power regulation range, spanning approximately -50 to 100 kW, as opposed to the traditional model's narrower range of -6 to 12 kW. This enhanced capability positions the novel model as a more adaptable solution to meet the power regulation demands

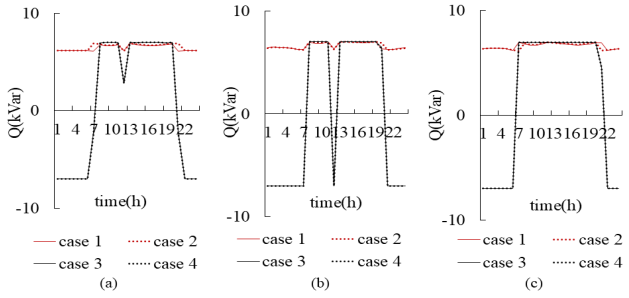

Fig. 7. Reactive power of BESS in four cases -(a) phase A (b) phase B (c) phase C

within the distribution network. The three-phase VSC-driven model operating in constant-value mode can deliver four times as much active power compared to the traditional model, thereby better showcasing the energy supply capacity of the BESS to the system. Furthermore, the BESS operating in charging/discharging mode varies according to load fluctuations, resulting in greater energy savings than constant-value mode.

Based on the images represented in Fig. 7, it can be deduced that the three-phase VSC-driven model's reactive power output remains relatively stable, whereas the traditional model's reactive power stabilizes only briefly, requiring power absorption from the system during early morning and nighttime hours. Compared with the conventional BESS, the three-phase VSC-driven BESS acts as an equivalent power source, which can supply reactive power to the load and improve the system's reactive power level better.

C. Voltage performance

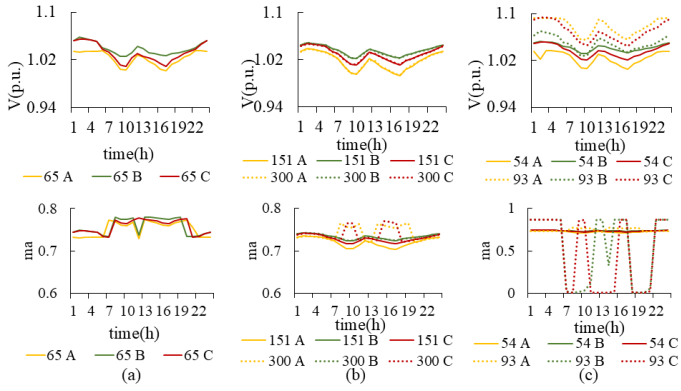

Fig. 8. Three-phase voltage and VSC's amplitude modulation index -(a) BESS (b) SOP1 (c) SOP2

As shown in the Fig. 8, bus voltages are analyzed to observe changes in voltage over a 24-hour period. With the regulation of BESS and SOP, the voltage remains generally stable within the specified range. During peak loads, there is a slight reduction in bus voltage, but it does not fall below the lower limit. When bus voltage decreases, the modulation factor increases accordingly to restore the voltage to its normal level. $m_a^{'}$ remains relatively constant when the voltage is in a stable state. However, because the $m_a^{'}$ is influenced not only by voltage but also by reactive power, there are significant fluctuations in the phase B and phase C of bus 93 to coordinate changes in reactive power in Fig.8 (c).

D. Evaluating the Efficacy of Progressive PSD Integration

TABLE IV
IMPACT OF INCREASING PSD INSTALLATIONS ON NETWORK LOSSES AND THREE-PHASE IMBALANCE

PSD number	0	2	4	6
Bus number	/	48,76	47,48,49,76	7,47, 48,49,65,76
Ploss(MW)	0.7302	0.7025	0.7021	0.7000
Improvement rate	/	3.79%	3.85%	4.14%
Imbalance Index(1E-2)	7.07	6.48	6.41	6.36

In evaluating the influence of PSD on network management, the table elucidates the correlation between the number of installed PSDs and improvements in both power losses and three-phase balance. With an escalating number of PSD installations, a tangible decrease in line losses is discernible. As TABLE IV underscores, the absence of PSDs yields a line loss of 0.7302 MW with a three-phase imbalance index of 7.07x10E-2. However, the integration of two PSDs, positioned at buses 48 and 76, translates to a 3.79% enhancement in power losses and a substantial drop in the imbalance index to 6.48x10E-2. The progression to four PSDs—sited at buses 47, 48, 49, and 76—affords a marginally superior 3.85% mitigation in losses, accompanied by an imbalance index of 6.41x10E-2. Remarkably, deploying six PSDs across buses 7, 47, 48, 49, 65, and 76 culminates in a 4.14% decrement in losses, further refining the balance to an index of 6.36x10E-2. However, the incremental benefits in line losses exhibit a diminishing trend with increasing PSD numbers. This nuance necessitates a judicious evaluation of economic and efficiency trade-offs when strategizing PSD deployments.

IV. CONCLUSION

This study emphatically showcases the benefits of embedding VSC technology in SOP models. The three-phase VSC-driven SOP significantly outperforms traditional SOP models, reducing line losses from 0.7382 to 0.7302 MW over 24 hours and improving the three-phase imbalance index from 8.58 to 7.07 (10E-2). These metrics affirm the superior efficiency and balance of three-phase VSC-driven modelling of SOP . Notably, enhancements in both SOP active and reactive power underscore the model's advantages in power quality management.

The research presents an insightful comparison between three-phase VSC-driven and traditional BESS models, underscoring transformative benefits, particularly with PSD integration. This synergy amplifies the BESS's adaptability with advanced VSC technologies, improving power quality and balance. Based on symmetrical SDP algorithm and convex relaxation, Benders decomposition is utilized to solve the mixed-integer programming for three-phase optimal power flow, which facilitates the resolution of the transformer tap

ratio and PSD's phase setting. This work not only elucidates the merits of employed three-phase devices but also propounds an innovative algorithmic route for system optimization, laying a solid foundation for future explorations aimed at refining electrical distribution networks' accuracy and efficiency.

REFERENCES

[1] D. Fan, H. Wang, F. Wang *et al.*, "Three-phase imbalance governance method for distribution network based on big data analysis," in *2021 IEEE 4th International Conference on Computing, Power and Communication Technologies (GUCON)*, 2021, pp. 1–6.

[2] C. Vidal, L. Tarisciotti, M. Díaz *et al.*, "Application of a single-phase matrix converter for electric vehicle charging," in *2022 IEEE Biennial Congress of Argentina (ARGENCON)*, 2022, pp. 1–7.

[3] S. Kjaer, J. Pedersen, and F. Blaabjerg, "A review of single-phase grid-connected inverters for photovoltaic modules," *IEEE Transactions on Industry Applications*, vol. 41, no. 5, pp. 1292–1306, 2005.

[4] X. Zeng, H. Zhai, M. Wang *et al.*, "A system optimization method for mitigating three-phase imbalance in distribution network," *International Journal of Electrical Power Energy Systems*, vol. 113, pp. 618–633, 2019. [Online]. Available: https://www.sciencedirect.com/science/article/pii/S0142061518339930

[5] S. Soltani, M. Rashidinejad, and A. Abdollahi, "Dynamic phase balancing in the smart distribution networks," *International Journal of Electrical Power Energy Systems*, vol. 93, pp. 374–383, 2017. [Online]. Available: https://www.sciencedirect.com/science/article/pii/S0142061516308870

[6] F. Ni, J. Q. Liu, F. Wei *et al.*, "Phase identification in distribution systems by data mining methods," in *2017 IEEE Conference on Energy Internet and Energy System Integration (EI2)*, 2017, pp. 1–6.

[7] S. Liu, X. Cui, Z. Lin *et al.*, "Practical method for mitigating three-phase unbalance based on data-driven user phase identification," *IEEE Transactions on Power Systems*, vol. 35, no. 2, pp. 1653–1656, 2020.

[8] O. Homaee, A. Najafi, M. Dehghanian *et al.*, "A practical approach for distribution network load balancing by optimal re-phasing of single phase customers using discrete genetic algorithm," *International Transactions on Electrical Energy Systems*, vol. 29, no. 5, p. e2834, 2019.

[9] X. Zeng, H. Zhai, M. Wang *et al.*, "A system optimization method for mitigating three-phase imbalance in distribution network," *International Journal of Electrical Power & Energy Systems*, vol. 113, pp. 618–633, 2019.

[10] S. Liu, Z. Lin, J. Li *et al.*, "Bi-level optimal placement model of phase switch devices for mitigating three-phase unbalance in low-voltage areas," *IEEE Transactions on Power Systems*, vol. 37, no. 4, pp. 3149–3152, 2022.

[11] F. Liang, J. Ni, H. Zhu *et al.*, "Optimal phase switch device placement scheme for low voltage distribution network considering load and renewable energy uncertainty," in *2022 Asia Power and Electrical Technology Conference (APET)*, 2022, pp. 157–160.

[12] C. E. Free and C. S. Aitchison, *Switches and Phase Shifters*, 2022, pp. 267–299.

[13] B. Liu, F. Geth, N. Mahdavi *et al.*, "Load balancing in low-voltage distribution networks via optimizing residential phase connections," in *2021 IEEE PES Innovative Smart Grid Technologies - Asia (ISGT Asia)*, 2021, pp. 1–5.

[14] S. Soltani, M. Rashidinejad, and A. Abdollahi, "Dynamic phase balancing in the smart distribution networks," *International Journal of Electrical Power & Energy Systems*, vol. 93, pp. 374–383, 2017.

[15] B. Liu, K. Meng, Z. Y. Dong *et al.*, "Unbalance mitigation via phase-switching device and static var compensator in low-voltage distribution network," *IEEE Transactions on Power Systems*, vol. 35, no. 6, pp. 4856–4869, 2020.

[16] A. Nakadomari, R. Shigenobu, and T. Senjyu, "Optimal control and placement of step voltage regulator for voltage unbalance improvement and loss minimization in distribution system," in *2020 IEEE REGION 10 CONFERENCE (TENCON)*, 2020, pp. 1013–1018.

[17] M. Chamana and B. H. Chowdhury, "Optimal voltage regulation of distribution networks with cascaded voltage regulators in the presence of high pv penetration," *IEEE Transactions on Sustainable Energy*, vol. 9, no. 3, pp. 1427–1436, 2018.

[18] J. Wang, N. Zhou, Y. Ran *et al.*, "Optimal operation of active distribution network involving the unbalance and harmonic compensation of converter," *IEEE Transactions on Smart Grid*, vol. 10, no. 5, pp. 5360–5373, 2019.

[19] M. Yao, I. A. Hiskens, and J. L. Mathieu, "Mitigating voltage unbalance using distributed solar photovoltaic inverters," *IEEE Transactions on Power Systems*, vol. 36, no. 3, pp. 2642–2651, 2021.

[20] J. Li, Z. Hai, Z. Shuai *et al.*, "Coordinated current and voltage unbalance mitigation in networked microgrids with aggregated pv systems," *IEEE Transactions on Power Systems*, vol. 38, no. 1, pp. 968–971, 2023.

[21] T.-W. Tsai, Y.-C. Li, C.-J. Yang *et al.*, "Per-phase active power distribution strategy for three-phase grid-tied inverters under unbalanced conditions without dc sources," *IEEE Journal of Emerging and Selected Topics in Power Electronics*, vol. 9, no. 6, pp. 6624–6636, 2021.

[22] A. Garcés, J. C. Castaño, and M. A. Rios, "Phase balancing in power distribution grids: A genetic algorithm with a group-based codification," *Handbook of Optimization in Electric Power Distribution Systems*, pp. 325–342, 2020.

[23] X. Jiang, Y. Zhou, W. Ming *et al.*, "An overview of soft open points in electricity distribution networks," *IEEE Transactions on Smart Grid*, vol. 13, no. 3, pp. 1899–1910, 2022.

[24] A. Tao, N. Zhou, Y. Chi *et al.*, "Multi-stage coordinated robust optimization for soft open point allocation in active distribution networks with pv," *Journal of Modern Power Systems and Clean Energy*, pp. 1–12, 2022.

[25] Z. Li, Z. Tang, W. Chao *et al.*, "Multi-objective supply restoration in active distribution networks with soft open points," in *2018 2nd IEEE Conference on Energy Internet and Energy System Integration (EI2)*, 2018, pp. 1–5.

[26] Z. Liu and L. Wang, "A robust strategy for leveraging soft open points to mitigate load altering attacks," *IEEE Transactions on Smart Grid*, vol. 13, no. 2, pp. 1555–1569, 2022.

[27] H. Ji, C. Wang, P. Li *et al.*, "Robust operation of soft open points in active distribution networks with high penetration of photovoltaic integration," *IEEE Transactions on Sustainable Energy*, vol. 10, no. 1, pp. 280–289, 2019.

[28] C. Lou, J. Yang, T. Li *et al.*, "New phase-changing soft open point and impacts on optimising unbalanced power distribution networks," *IET generation, transmission & distribution*, vol. 14, no. 23, pp. 5685–5696, 2020.

[29] C. Lou, J. Yang, E. Vega-Fuentes *et al.*, "Multi-terminal phase-changing soft open point sdp modeling for imbalance mitigation in active distribution networks," *International Journal of Electrical Power & Energy Systems*, vol. 142, p. 108228, 2022.

[30] X. Cui, G. Ruan, F. Vallée *et al.*, "A two-level coordination strategy for distribution network balancing," *IEEE Transactions on Smart Grid*, pp. 1–1, 2023.

[31] L. Min, J. Yang, C. Lou *et al.*, "Phase-changing control for three-phase four-wire back-to-back vsc based soft open points," in *11th International Conference on Renewable Power Generation - Meeting net zero carbon (RPG 2022)*, vol. 2022, 2022, pp. 110–114.

[32] T. Wu, Y. J. Zhang, and X. Tang, "A vsc-based bess model for multi-objective opf using mixed integer socp," *IEEE Transactions on Power Systems*, vol. 34, no. 4, pp. 2541–2552, 2019.

[33] T. Wu, C. Zhao, and Y.-J. A. Zhang, "Distributed ac-dc optimal power dispatch of vsc-based energy routers in smart microgrids," *IEEE Transactions on Power Systems*, vol. 36, no. 5, pp. 4457–4470, 2021.

[34] Z. Wang, D. S. Kirschen, and B. Zhang, "Accurate semidefinite programming models for optimal power flow in distribution systems," *arXiv preprint arXiv:1711.07853*, 2017.

[35] G. Paap, "Symmetrical components in the time domain and their application to power network calculations," *IEEE Transactions on Power Systems*, vol. 15, no. 2, pp. 522–528, 2000.

[36] P. M. Anderson, *Analysis of faulted power systems*. John Wiley & Sons, 1995, vol. 11.

[37] M. Abdel-Akher and K. M. Nor, "Fault analysis of multiphase distribution systems using symmetrical components," *IEEE Transactions on Power Delivery*, vol. 25, no. 4, pp. 2931–2939, 2010.

[38] B. Kazemtabrizi and E. Acha, "An advanced statcom model for optimal power flows using newton's method," *IEEE Transactions on Power Systems*, vol. 29, no. 2, pp. 514–525, 2014.

[39] I. Alsaleh, L. Fan, and M. Ma, "Mixed-integer sdp relaxation-based volt/var optimization for unbalanced distribution systems," in *2019 IEEE Power Energy Society General Meeting (PESGM)*, 2019, pp. 1–5.

[40] I. Alsaleh and L. Fan, "Multi-time co-optimization of voltage regulators and photovoltaics in unbalanced distribution systems," *IEEE Transactions on Sustainable Energy*, vol. 12, no. 1, pp. 482–491, 2021.

[41] R. Rahmaniani, T. G. Crainic, M. Gendreau *et al.*, "The benders decomposition algorithm: A literature review," *European Journal of Operational Research*, vol. 259, no. 3, pp. 801–817, 2017.

[42] A. M. Geoffrion, "Generalized benders decomposition," *Journal of optimization theory and applications*, vol. 10, pp. 237–260, 1972.
[43] M. Paredes, L. S. A. Martins, S. Soares *et al.*, "Benders' decomposition of the unit commitment problem with semidefinite relaxation of AC power flow constraints," *Electric Power Systems Research*, vol. 192, p. 106965, 2021. [Online]. Available: https://www.sciencedirect.com/science/article/pii/S037877962030763X
[44] A. Soares, A. Street, T. Andrade *et al.*, "An integrated progressive hedging and benders decomposition with multiple master method to solve the brazilian generation expansion problem," *IEEE Transactions on Power Systems*, vol. 37, no. 5, pp. 4017–4027, 2022.
[45] B. Zhang, L. Zhang, W. Tang *et al.*, "Optimal planning of hybrid ac/dc low-voltage distribution networks considering dc conversion of three-phase four-wire low-voltage ac systems," *Journal of Modern Power Systems and Clean Energy*, vol. 12, no. 1, pp. 141–153, 2024.
[46] P. Li, H. Ji, C. Wang *et al.*, "Coordinated control method of voltage and reactive power for active distribution networks based on soft open point," *IEEE Transactions on Sustainable Energy*, vol. 8, no. 4, pp. 1430–1442, 2017.
[47] C. Wang, G. Song, P. Li *et al.*, "Optimal siting and sizing of soft open points in active electrical distribution networks," *Applied Energy*, vol. 189, pp. 301–309, 2017. [Online]. Available: https://www.sciencedirect.com/science/article/pii/S0306261916318499
[48] J. Lofberg, "Yalmip : a toolbox for modeling and optimization in matlab," in *2004 IEEE International Conference on Robotics and Automation (IEEE Cat. No.04CH37508)*, 2004, pp. 284–289.
[49] P. Li, H. Ji, C. Wang *et al.*, "Optimal operation of soft open points in active distribution networks under three-phase unbalanced conditions," *IEEE Transactions on Smart Grid*, vol. 10, no. 1, pp. 380–391, 2019.

Chengwei Lou received the B.S. degree and the M.E. degree in Electrical Engineering and Automation from China Agricultural University, Beijing, China, in 2016 and 2019. He received the Ph.D. degree in Electrical Engineering at the University of Glasgow in 2022. He is currently an Associate Professor with College of Information and Electrical Engineering at the China Agricultural University, Beijing, China. His current research interests include power distribution system modelling and optimization.

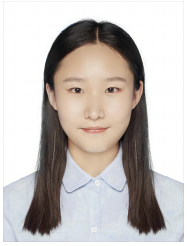

Ran Zhao is currently working toward the M.E. degree in electrical engineering at China Agricultural University, Beijing, China. Her main research interests include resilience enhancement in hybrid AC/DC distribution network and active distribution networks.

Hangxing Zhang is currently pursuing an M.E. degree in electrical engineering at China Agricultural University, Beijing, China. His main research interests include the applications of Benders decomposition algorithms in electric vehicles.

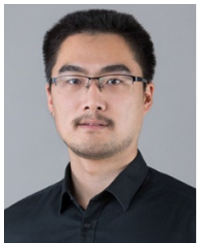

Lu Zhang (Senior Member, IEEE) was born in Beijing, China on February 10, 1990. He received the B.S. degree in electrical engineering and the Ph.D. degree in agricultural electrification and automation from China Agricultural University, Beijing, China, in 2011 and 2016, respectively.

From 2017 to 2019, he was a Postdoc with the Department of Electrical Engineering, Tsinghua University, Beijing, China. He is currently a Professor with the College of Information and Electrical Engineering, China Agricultural University, Beijing, China. His main research interests include hybrid AC/DC distribution network, renewable energy generation, and active distribution networks.

Wei Tang (Member, IEEE) received the B.S. degree in electrical engineering from the Huazhong University of Science and Technology, Wuhan, China, in 1992, and the Ph.D. degree in electrical engineering from the Harbin Institute of Technology, Harbin, China, in 1998.

From 1998 to 2000, she was a Postdoc with Harbin Engineering University, Harbin, China. She is currently a Professor with the College of Information and Electrical Engineering, China Agricultural University, Beijing, China. Her research interests include distribution network economic and security operation, distributed generation, and active distribution network.

Jin Yang (Senior Member, IEEE) received the Ph.D. from University of Glasgow, UK, in 2011. Currently, he is a Reader in James Watt School of Engineering, University of Glasgow. His research interests include renewable distributed energy resources and their impacts on the power distribution networks, with flexible and innovative operational technologies.

Linjuan Zhang is currently working at the State Grid HeNan Economic Research Institute, Zhengzhou. Her research focuses on the orderly charging of electric vehicles and charging networks.